Fabrication, Characterization and Index Profile Modeling of High-Damage Resistance Zn-Diffused Waveguides in Congruent and MgO: Lithium Niobate

W. M. Young, M. M. Fejer, M. J. F. Digonnet, A. F. Marshall, and R. S. Feigelson

Abstract— **A study of the fabrication and optical properties of planar waveguides fabricated in MgO:$LiNbO_3$ and $LiNbO_3$ substrates by diffusion of a ZnO film is presented. Transmission electron microscopy was used to show that using ZnO instead of metallic zinc as a source, and maintaining the ZnO film thickness below a prescribed value, greatly reduces second phase precipitation and produces usable waveguides. Dopant and refractive index profiles were characterized by electron microprobe analysis and interference microscopy, respectively. The dependence of the Zn diffusion coefficient on temperature and the dependence of the refractive-index change on Zn concentration are inferred from these measurements. A simple model is also reported which predicts the index profile of the waveguide given the film thickness, diffusion time and temperature. The validity of the model is demonstrated by comparison between calculated profiles and profiles measured by prism coupling and IWKB analysis.**

I. Introduction

OPTICAL waveguides in lithium niobate ($LiNbO_3$) have been widely studied for applications including telecommunication systems, nonlinear optics and fiber sensors. To date the two most widely used waveguide fabrication processes are titanium diffusion and proton-exchange (PE) [1], [2]. Both processes yield waveguides with low propagation loss, typically lower than 0.5 dB/cm [2], [3]. However, neither method produces waveguides with ideal performance for all applications. Ti-diffused waveguides in both $LiNbO_3$ and MgO:$LiNbO_3$ guide both polarizations but suffer from photorefractive damage even at wavelengths as long as 0.85 μm [4], [5]. On the other hand, PE waveguides are much more resistant to photorefractive damage but guide only the extraordinary polarization.

The objective of this work was to develop a new type of waveguide in $LiNbO_3$ which can guide both polarizations and exhibit high resistance to photorefractive damage. The current model for the photorefractive effect involves a refractive-index perturbation due to an interaction between the electrooptic effect and the local electric field created by charge separation under visible laser illumination [6]. Since the charge generation and trapping centers are strongly related to dopant valence state, we speculated that cation dopants with a single valence state less than or equal to 2, such as Mg^{+2} and H^{+}, will have similar effects on photorefractive damage. This hypothesis was based on the experimental observations that both Mg^{+2} and H^{+} reduce the photorefractive damage [7], [8], while cation dopants with multivalent states or a valence state greater than or equal to 3, such as Fe^{+3}/Fe^{+2}, Nd^{+3} and Ti^{+4}, increase the photorefractive damage [9], [10].

In this work, Zn was chosen as a dopant because it matches the requirements predicted from the above arguments. In a recent article, we reported the fabrication and optical properties of planar waveguides made by the diffusion of ZnO into both $LiNbO_3$ and MgO:$LiNbO_3$. Waveguides made in the latter material guide both polarizations, although with a substantial difference in index profile, and have propagation losses in the range of 0.3 to 1.2 dB/cm. They also exhibit no photorefractive in-plane scattering up to 90 kW/cm^2 at 514.5 nm, which is one of the highest values reported in the literature [11].

In this paper we present detailed material and optical studies of Zn-diffused waveguides in both MgO:$LiNbO_3$ and $LiNbO_3$. Fabrication conditions required to obtain low loss waveguides are identified, in particular to avoid the formation of second phase precipitation of $LiZnNbO_4$ and surface degradation. We report measurements by electron microprobe analysis of the dopant distribution in Zn-diffused lithium niobate waveguides, as well as optical characterization of their index profiles. This data is used to obtain values of the diffusion coefficient of Zn in congruent and MgO-doped $LiNbO_3$, their dependence on temperature, and the relationship between the refractive-index change and the Zn concentration. We also introduce a simple model, employing the diffusion and fabrication parameters, to calculate the dopant concentration profile, and from it the index profile of the waveguide. Comparison between the predictions of this model and the measured waveguide index profiles establishes the validity of this model.

II. Fabrication

A. Experimental Procedures

To prepare the Zn-diffused samples, a ZnO film was first sputtered onto the $LiNbO_3$ substrates. The dimensions of the substrates used to produce waveguides were 20 × 6 × 2 mm for MgO:$LiNbO_3$ and 20 × 6 × 1 mm for $LiNbO_3$. Diffusion studies for both materials were carried out on 6 × 4 × 1

Manuscript received November 25, 1991; revised March 27, 1992.

W. M. Young and R. S. Feigelson are with the Department of Materials Science and Engineering, Stanford University, Stanford, CA 94305.

M. M. Fejer and M. J. F. Digonnet are with the Edward L. Ginzton Laboratory, Stanford University, Stanford, CA 94305.

A. F. Marshall is with the Center for Materials Research, Stanford University, Stanford, CA 94305.

IEEE Log Number 9201292.

mm substrates. During diffusion, the samples were placed on platinum foil stands in the center of a covered alumina boat filled with congruent lithium niobate powder. The purpose of the powder is to suppress the net transport of Li ions in or out of the lithium niobate crystal [12]. To control the Li_2O vapor pressure in the vicinity of the $LiNbO_3$, we used a mass of powder substantially larger than that of the sample (about 13 g versus less than 0.6 g). The alumina boat was placed in the center of an alumina process tube, closed at both ends with alumina caps, which, in turn, was placed in a tube furnace for diffusion at elevated temperatures in dry air [13]. The temperature difference between the control thermocouple and a monitor thermocouple at the sample location was less than 0.5°C. In the text the quoted temperatures are provided by the control thermocouple. The thermal cycle, carried out in dry air, typically involved heating at about 8°C/min up to the diffusion temperature of 1000–1100°C, diffusion for typically less than 1 hour, and cooling at an initial rate of 10°C/min.

Fig. 1. Bright-field TEM photograph of a Zn-diffused congruent $LiNbO_3$ surface showing a precipitate (400-nm ZnO diffused at 1000°C for 1 hour).

B. Surface Roughness

To produce low scatter loss waveguides it is crucial that the surface quality be not degraded by the diffusion process. In our initial diffusion experiments the surfaces of all the samples were translucent after diffusion. Similar observations of surface degradation resulting from the diffusion of metallic Zn into $LiNbO_3$ were previously reported by Yoon *et al.* [14]. Based on the ZnO-Li_2O-Nb_2O_5 pseudo-ternary phase diagram [15], we speculated that the surface roughening originated from the formation of a new phase on the substrate surface. The phase diagram suggests that $LiZnNbO_4$ is a stable compound, which could therefore form near the sample surface and degrade its quality. For comparison, in the case of the diffusion of Ti in lithium niobate, the TiO_2-Li_2O-Nb_2O_5 pseudo-ternary phase diagram indicates that TiO_2 and $LiNbO_3$ can coexist in equilibrium at temperatures up to 1100°C [16]. Consequently, during the diffusion of Ti some metastable phases may form at elevated temperature but they will dissolve into lithium niobate over the course of the fabrication process [17], [18].

Transmission electron microscopy (TEM) confirmed the presence of $LiZnNbO_4$ precipitates near the diffusion surface. Fig. 1 shows a bright field TEM picture of the substrate surface after diffusion of a 400 nm-thick film of ZnO at 1000°C for 1 h. Isolated second phases, on the order of a few microns in size, were observed across the surface of the substrate. Energy-dispersive spectrometry confirmed that these precipitates contained high Zn concentration. The electron diffraction pattern of the precipitate has been identified as $LiZnNbO_4$. Fig. 2 shows the electron diffraction pattern of the substrate (Fig. 2(a)) and of the precipitate (Fig. 2(b)). The lattice constants measured in Fig. 2(b) are consistent with documented values for $LiZnNbO_4$. The precipitates are always in a $\langle 201 \rangle$ orientation and have a specific in-plane alignment with respect to the $\langle 001 \rangle$ $LiNbO_3$ substrate. The $\{100\}$ and $\{112\}$ planes of the precipitates are parallel to the $\{10.0\}$ planes of the substrate. For the $LiZnNbO_4$ structure, the angle between the two sets of planes is 59.2°, whereas the in-plane angles for <001> $LiNbO_3$ are 60°. The reflections from the precipitate (Fig. 2(b)) can be superimposed on the substrate (Fig. 2(a)) which indicates that the precipitates are slightly strained to give better alignment with the substrate. The orientation relationship between precipitates and substrate also gives three variants for the orientation of the precipitates and all of these can be observed within a given precipitate region. These results strongly suggest that a $LiZnNbO_4$ precipitate formed epitaxially on the top surface of the waveguide during Zn diffusion. These isolated precipitates were probably responsible for the prohibitively high loss observed in early waveguides.

There are at least two approaches to eliminate these second phase precipitates: 1) synthesize the dopant source from a composition within the $LiNbO_3$-$ZnNb_2O_6$-$ZnLiNbO_4$ tie triangle where $LiNbO_3$ is in equilibrium with quaternary Zn containing compounds or 2) find a set of parameters for ZnO diffusion which avoids the precipitation. The first approach would involve an in-depth study of dopant synthesis techniques and

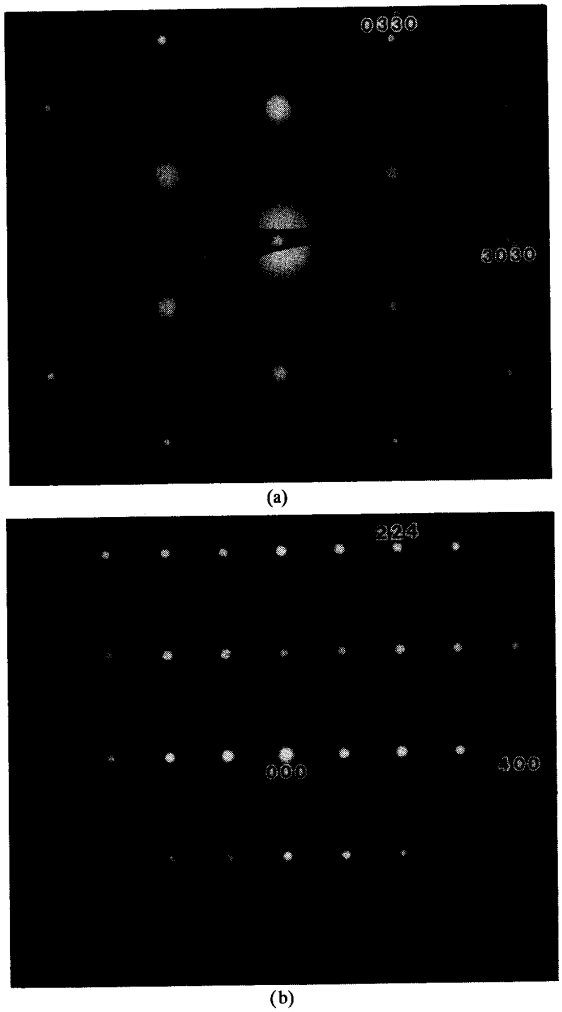

Fig. 2. Electron diffraction patterns from the $LiNbO_3$ substrate (a) and precipitate (b) measured from the sample shown in Fig. 1. The reflections indexed {30.0} planes from the substrate $LiNbO_3$ in Fig. 2(a) matches the {400} and {224} planes from the precipitate in Fig. 2b, indicating epitaxial relationship between the substrate and the precipitate.

compositional control during deposition of the source on the substrate. As a result the second alternative appeared to be a more desirable approach for establishing the usefulness of Zn-diffused $LiNbO_3$ waveguides.

The key point in the second approach is to avoid any kinetic paths leading to compound formation. To this end ZnO was chosen instead of metallic zinc to avoid unnecessary metal oxidation which may enhance the formation of the intermediate phase [19]. We also found that an important parameter controlling the formation of the precipitate is ZnO film thickness. We established experimentally that compound formation is greatly reduced, if not completely eliminated, when the film thickness is kept below some critical value. This critical thickness is approximately 160 nm for MgO:$LiNbO_3$ and 100 nm for $LiNbO_3$. No precipitate was observed in these materials with thicknesses of ZnO smaller than these values and for diffusion temperatures anywhere between 1000 and 1100°C. Satisfying the thickness condition was found to be essential to maintaining a good surface quality and producing low loss waveguides. By appropriate selection of the diffusion time and temperature (between 1000 and 1100°C for MgO:$LiNbO_3$ and around 1000°C for congruent $LiNbO_3$), the Zn concentration in the diffused region is high enough (typically 2–3 mol%) to provide good optical confinement, and yet low enough to maintain a good surface quality.

III. Dopant And Diffusion Characterization

Electron microprobe analysis (EMPA) to measure the dopant profiles in the Zn-diffused region required longer diffusion times (1–10h) and thicker ZnO films (0.4–1.0 m) than those used for the fabrication of waveguides. This was necessary so that high enough Zn concentrations would be present over greater depths to permit accurate EMPA measurement. Prior to characterization, a Zn-diffused sample was first sandwiched between two glass slides, then cut into two pieces. Each piece was polished at both ends, perpendicular to the diffusion surface. One piece was used for EMPA measurements, the other for Mach–Zehnder interference microscope measurements, as described in Section IV. The glass slides were used to prevent rounding of the edges of the diffused region during polishing, which would otherwise upset EMPA and microscopy measurements.

An example of dopant profile is shown in Fig. 3 for an x-cut MgO:$LiNbO_3$ substrate after diffusion of a 200-nm ZnO film at 1000°C for 10 h. For all diffused samples studied here the ZnO film was not completely depleted at the end of the diffusion process. This assumption was checked by integrating the measured dopant profile along the depth of the diffused region to obtain the total amount of Zn present in the sample, and comparing it to the amount of Zn initially contained in the film. It is well known from diffusion theory that when the film is undepleted (and the diffusion coefficient is independent of concentration) the profile is a complementary error function (erfc). This is in agreement with measured profiles, as illustrated by theoretical fit of the experimental profile to an erfc plot in Fig. 3. Consequently, the diffusion coefficient D was obtained by fitting each measured dopant profile with an erfc function.

Table I lists the values of D obtained from a total of 10 samples in 3 different types of substrates (z- and x-cut MgO:$LiNbO_3$ and z-cut congruent $LiNbO_3$) processed at temperatures between 900 and 1100°C. For short diffusion times, typically 1 hour or less, a nonnegligible amount of diffusion takes place during both the heating and cooling parts of the cycle. This was taken into account in correcting the measured diffusion coefficients by first estimating $D(T)$, without applying any corrections, for samples diffused at different temperatures. From these values the amount of diffusion occurring during heating and cooling was evaluated, assuming an exponential dependence $D(T)$, which provided a second, more accurate value of $D(T)$. This process was iterated 2 or 3 times until it converged to constant values. Table I lists both the uncorrected and the corrected values of D. Error bars were obtained from the average of several EMPA scans, typically

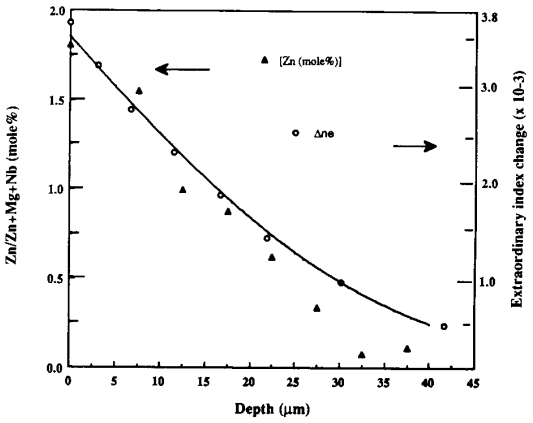

Fig. 3. Extraordinary refractive index (open circles) and Zn dopant (triangles) profiles of an x-cut MgO:$LiNbO_3$ substrate after diffusion of a 200-nm ZnO film at 1000°C for 10h. The solid line is a complementary error function fitted to the experimental concentration profile.

TABLE I
ZN DIFFUSION COEFFICIENTS FOR DIFFERENT TEMPERATURES AND SUBSTRATES. THE CORRECTED D ACCOUNTS FOR THE CONTRIBUTION OF FINITE DIFFUSION DURING WARMING AND COOLING.

Samples	Temp.	Time	ZnO thickness	$D(\mu m^2/h)$	D(corrected, $\mu m^2/h$)
MgO:$LiNbO_3$ z-cut	1100°C	1.4 h	160 nm	140±10	119±8
"	1100°C	10 h	160 nm	24.8±2	24.3±2
"	950°C	10 h	1 μm	8.7±2	8.5±2
"	900°C	100 h	1 μm	1.9±0.3	1.9±0.3
MgO:$LiNbO_3$ x-cut	1100°C	1 h	200 nm	138±12	110.8±10
"	1000°C	10 h	200 nm	27±6	26.4±6
"	900°C	10 h	200 nm	2.4±0.2	2.4±0.2
$LiNbO_3$ z-cut	1100°C	1 h	1 μm	280±26	230±21
"	1000°C	4 h	1 μm	35.5±4	34±4
"	950°C	10 h	1 μm	9.6±1.4	9.4±1.4

2 to 4, taken at different positions on the same sample. They reflect some compositional nonuniformity across the samples as well as measurement uncertainties. Comparing the error bars of samples fabricated under similar conditions, it appeared that the dopant profile was more uniform for thinner ZnO films. This may be an important consideration in the preparation of waveguides with uniform index profiles.

The samples used for D(T) measurements, which were fabricated with thick ZnO films, exhibit erfc profiles with a depth that varies as the square root of the diffusion time. This is an indication that, while second phase precipitation was present in these samples, the formation of this phase is clearly not a significant limiting step in the Zn transport process, at least within the accuracy of our measurements. Instead, the rate limiting step is diffusion of Zn in lithium niobate. The values of the diffusion coefficients $D(T)$ measured from the diffusion of thick films should be applicable to the analysis of the diffusion of thin films necessary for waveguide fabrication.

Fig. 4 shows the Arrhenius plot ($\ln D$ versus $1/T$) for x-cut and z-cut MgO:$LiNbO_3$. The dependence is linear between 900°C to 1100°C, as expected. The activation energy inferred from the slope of the curve is $E_0 = 2.72 \pm 0.2$ eV. Within our measurement accuracy, we did not detect diffusion anisotropy in MgO:$LiNbO_3$, as shown by the results of Fig. 4. Fig. 5 shows a similar curve for z-cut $LiNbO_3$. The points falls on a straight line between the 950 and 1100°C, with an activation energy of $E_0 = 3.02 \pm 0.3$ eV. This measurement was not carried out for x-cut $LiNbO_3$. These high activation energies suggest that the diffusion mechanism of Zn in $LiNbO_3$ favors substitutional over interstitial mechanisms, as the latter type is usually characterized by a smaller activation energy [20]. The diffusion of Zn is much faster than that of Ti, and fabrication times are correspondingly shorter.

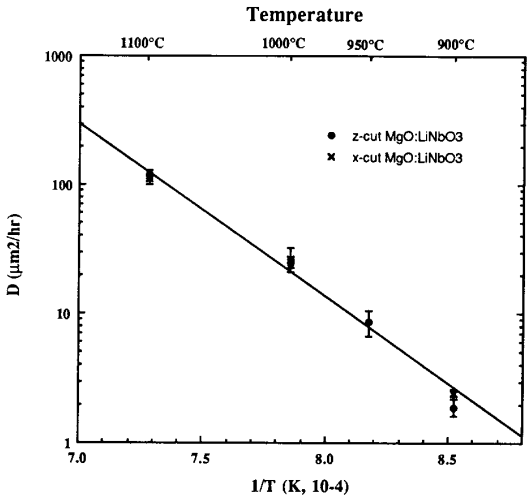

Fig. 4. The Arrhenius ($\ln D$ versus $1/T$) plot for the diffusion of ZnO, under conditions specified in the text, in z-cut and x-cut MgO:$LiNbO_3$ between 900 and 1100°C.

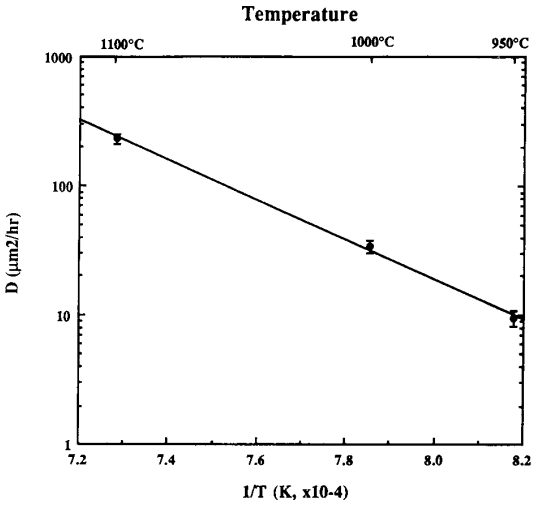

Fig. 5. Same as Fig. 4, for Zn diffused z-cut $LiNbO_3$ between 950 and 1100°C.

IV. Index Characterization and Index-Dopant Relationship

The index profiles, later used to establish the relationship between the refractive-index change and the dopant concentration, were obtained by interference microscopy. For this purpose, the samples were sliced and polished as described in Section III. The samples, typically 1-mm thick, were placed in one of the arms of a Mach–Zehnder interference microscope operated with a 632.8 nm He–Ne laser, such that the light traveled through the length of the diffused region. The microscope produced a magnified image of the diffused region on which refractive index changes were mapped as distortions of the interference fringe pattern. Index profiles were inferred from the number of fringes of distortion at different positions along the depth of the diffused region. This method was generally preferred over prism coupling and IWKB analysis [21] because it is more easily applied to small samples with rough surfaces. In cases where the two methods were compared, the profiles agreed within 20%.

Since the refractive-index change was typically small (less than 0.005), potential changes in the index from sources other than the Zn dopant had to be carefully evaluated. These sources include impurities in the ZnO film or in the furnace, departure from parallelism in the sample end faces, and Li in-or-out diffusion, which is known to change the extraordinary refractive index of lithium niobate [22]. To make sure that no other process was affecting the index, a monitor sample of congruent $LiNbO_3$ (with no ZnO film) was routinely placed in the furnace and checked for contaminants by *X*-ray photoelectron spectrometry (XPS) and for index change by Mach–Zehnder interference microscopy. Within the resolution of both methods, we observed no detectable furnace contamination or Li in-or-out diffusion in the monitor sample. A slight wedge between the sample end faces and residual rounding of the edges can also be a source of error when interpreting the fringe pattern obtained from Mach–Zehnder interference microscopy. Michelson interference microscopy indicated that effects of rounding were negligible and that the contribution of any wedge to the measured refractive-index change was less than 1×10^{-4}.

Studies of index profiles were carried out on samples diffused at 1100 and 1000°C for both *x*- and *z*-cut MgO:$LiNbO_3$, and at 1000°C for *z*-cut $LiNbO_3$. A typical index profile is shown in Fig. 3 for the extraordinary index of *x*-cut MgO:$LiNbO_3$. We estimate the error on the index measurement to be about 5×10^{-4}, and the spatial resolution to be 2–3 μm. The index change is maximum at the surface and equal to 3.7×10^{-3}. The half-maximum depth of the index profile is about 16 μm. The measured refractive-index profile resembles the Zn concentration profile measured in the same sample (see Fig. 3). Fig. 6 shows the dependence of the index change on the Zn concentration taken from the data of Fig. 3. The slope of a linear fit to the data is about $1.90 \pm 0.1 \times 10^{-3}$ per Zn mol%. Fig. 7 shows a similar curve for another sample, also fabricated in *x*-cut MgO:$LiNbO_3$ but at 1100°C. For this particular sample, the index change appears to vary somewhat nonlinearly with Zn concentration. A linear fit to the data gives

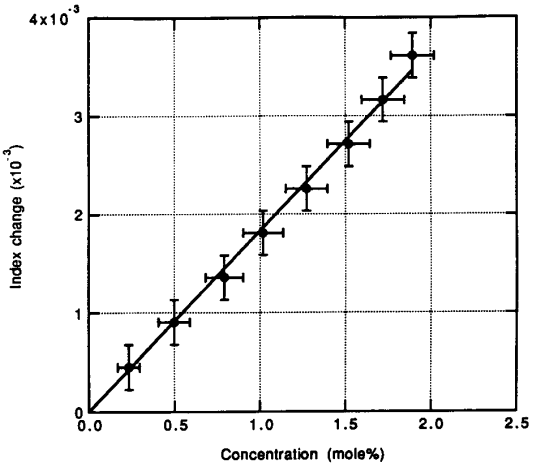

Fig. 6. The extraordinary index change as a function of Zn concentration measured in an *x*-cut MgO:$LiNbO_3$ sample after diffusion of a 200-nm ZnO film at 1000°C for 10h.

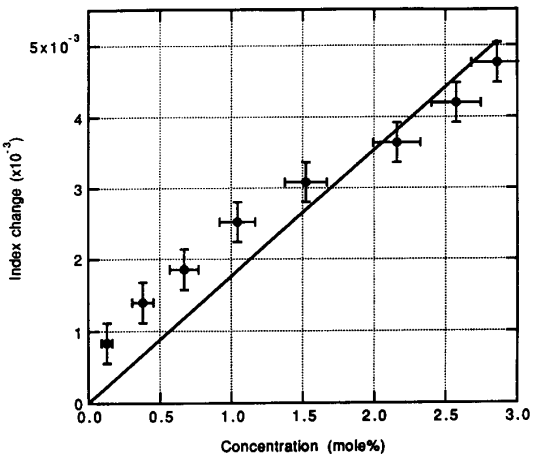

Fig. 7. Same as Fig. 6, but for diffusion at 1100°C for 1 h.

a slope of about $1.77 \pm 0.12 \times 10^{-3}$ per Zn mol%. More study needs to be done to define this dependence more precisely.

Table II summarizes the index change per Zn mol% measured on several samples representing a variety of materials, orientations and fabrication conditions. In both *x*- and *z*-cut MgO:$LiNbO_3$, the extraordinary index change is greater for diffusion at 1000°C than at 1100°C. For a given material the index change appears to depend only slightly on the substrate orientation and diffusion temperature. These conclusions are based on a limited number of samples, and should be considered as tentative.

For MgO:$LiNbO_3$ only the extraordinary index Δn_e was studied, as the ordinary index change Δn_o is generally too small to be measured accurately by interference microscopy, but was estimated to be on the order of 1/4 to 1/5 the value of Δn_e. The ordinary modes were successfully excited by end-firing [11] but not by prism coupling, at least in *x*-cut samples, so that n_o could not be measured by this method either.

TABLE II
THE INDEX CHANGE PER ZN CONCENTRATION FOR DIFFERENT MATERIALS, ORIENTATIONS AND TEMPERATURES.

Samples	Temp.	Time	ZnO thickness	Index change/[Zn mol%]
1.MgO:$LiNbO_3$,*x*-cut	1100°C	1 h	200 nm	$1.77\pm0.12\times10^{-3}$ (Δn_e)
2. "	1000°C	10 h	"	$1.83\pm0.02\times10^{-3}$ (Δn_e)
3.MgO:$LiNbO_3$,*z*-cut	1100°C	1.4 h	160 nm	$1.22\pm0.04\times10^{-3}$ (Δn_e)
4. "	1000°C	10 h	"	$1.90\pm0.10\times10^{-3}$ (Δn_e)
5. $LiNbO_3$,*z*-cut	1000°C	4 h	200 nm	$0.72\pm0.03\times10^{-3}$ (Δn_o)

For congruent $LiNbO_3$ the ordinary modes were easily excited by prism coupling. On the other hand the extraordinary modes were successfully excited by end firing but not by prism coupling. We also observed that the extraordinary index change is a nonmonotonic function which presents one or more extrema depending on the processing conditions. This behavior, which we believe may be related to local variations in lithium concentration, could be at the origin of the difficulty in prism coupling into this polarization. More studies are needed to elucidate this effect, which could be of interest to produce buried waveguides. This situation should be kept in mind when dealing with congruent $LiNbO_3$.

V. COMPARING CALCULATED AND MEASURED INDEX PROFILES

For the purpose of waveguide design, it would be useful to be able to predict the index profile of a waveguide from the fabrication conditions, i.e., from the film thickness, diffusion temperature, diffusion time, and the substrate material and orientation. To address this issue, we computed the concentration profile from diffusion theory, then multiplied this profile by the factor $\Delta n/[Zn]$ (the measured ratio of index change Δn to zinc concentration [Zn] listed in Table II). We present results for Zn:$LiNbO_3$ in this section. The index profiles predicted are shown to agree within 30% error with the profiles measured from prism coupling and IWKB analysis.

We considered the problem of one-dimensional diffusion of species A into solid B, with the assumption that (1) the solid solubility of A in B exists and is equal to C_o, and (2) the diffusion coefficient of A into B is independent of concentration. We also assume that as long as the film is not depleted, the dopant concentration at the surface of solid B is pinned at the value of the solid solubility C_o. This approximation for diffusion of thin ZnO films neglects the initial kinetics associated with dissolving Zn into $LiNbO_3$, but predicts results for waveguide samples with reasonable accuracy. Detailed modeling of the kinetic process is beyond the scope of this work. As discussed in Section II-B, in the present study this last assumption only applies when the ZnO film does not exceed a prescribed thickness. In this case it is well known that the solution of the diffusion equation is a complementary error function (erfc) [23], which can be written as:

$$c(x,t) = C_0 \mathrm{erfc}\left[\frac{x}{4Dt}\right] \qquad (t \le t_1) \tag{1}$$

where t is the total diffusion time and x is the depth measured from the diffusion surface (i.e., the original interface between species A and B). This solution applies only until the film is completely depleted, which first occurs at time $t = t_1$. The time t_1 is given by mass conservation, i.e., at $t = t_1$ the amount of material diffused into the solid per unit area is equal to the amount of material per unit area present in the film at time $t = 0$. Integration in x of (1) yields:

$$t_1 = \left(\frac{\kappa d}{1.128 C_0}\right)^2 \left(\frac{1}{D}\right) \tag{2}$$

where C_0 is expressed in mole%, d is the initial film thickness, and κ is given by:

$$\kappa = \frac{\rho_A}{\rho_B}\frac{M_B}{M_A}N \tag{3}$$

ρ_A and ρ_B are the density of species A and B, respectively, M_A and M_B are their respective molecular weight, and N is the number of ions per molecule. For the case under study N=1 and $\kappa = 2.23$.

For $t > t_1$, the solution of the diffusion equation is known to be:

$$c(x,t_2) = \frac{C_0}{\sqrt{4\pi D t_2}} \int_0^\infty \left(\frac{x'}{\sqrt{4Dt_1}}\right)\left[e^{-\frac{(x-x')^2}{4Dt_2}} + e^{-\frac{(x+x')^2}{4Dt_2}}\right] dx' \qquad (t \ge t_1) \tag{4}$$

where $t_2 = t - t_1$. In general, this solution can not be cast in a simple closed form expression and the integral has to be calculated numerically. As is well known, for $t_2 \gg t_1$ this solution approaches a Gaussian given by:

$$c(x,t_2) = \frac{\kappa d}{\sqrt{\pi D(t_1+t_2)}} e^{-\frac{x^2}{4D(t_1+t_2)}} \qquad (t_2 \ge t_1) \tag{5}$$

The 1/e width in (5) is $w_G = 4D\sqrt{(t_1+t_2)}$. The exact solution (4) converges toward the approximate solution fairly rapidly. For $t_2 = t_1$ the exact width differs from the approximate width w_G by only 11%, and for $t_2 = 4t_1$ by less than 4%. In practical diffusion runs, t_2 is usually longer than t_1, so that (5) provides a convenient and accurate approximation of the dopant profile.

The solid solubilities of Zn in $LiNbO_3$ and MgO:$LiNbO_3$ are necessary inputs for this calculation. In an ideal system, we would expect the solid solubility to depend on temperature, but at a given temperature the Zn concentration at the surface should be pinned at that value as long as the film is undepleted. In the Zn:$LiNbO_3$ system, in which the ZnO is not in thermodynamic equilibrium with the substrate materials, we obtained an effective solid solubility by measuring the Zn surface concentration with EMPA in several waveguides (with no detectable second phase precipitation, i.e., starting from ZnO film thicknesses smaller than the bounds specified in Section II-B). For a given temperature and substrate material,

the highest measured value provided a lower bound value of the solid solubility. For example, in a waveguide fabricated at 1100°C in x-cut MgO:$LiNbO_3$ the highest Zn surface concentration was equal to 3.5 ± 0.6 mole%. We assume C_o takes this value for all temperatures between 1000 to 1100°C, as no data was available for 1000°C. For $LiNbO_3$, the highest surface concentration observed and the value of C_o used was 5.4 ± 0.5 mole%. These two values were consistent with mass conservation, assuming that the film was just depleted at the end of these runs.

The diffusion temperature profile $T(t)$ is not rectangular in practice, as assumed in the model. Instead, the furnace is gradually heated to the diffusion temperature T_0, the temperature is then maintained at T_0 for a duration t, and finally the furnace is gradually cooled down. As mentioned earlier, a finite amount of diffusion takes place during heating and cooling cycles. The real cycle can be replaced by an equivalent rectangular cycle (i.e., with infinitely fast heating and cooling) producing the same amount of diffusion, provided time t is replaced by an equivalent diffusion time t_{eff} which can be shown to be given by:

$$t = t + \frac{kT_0^2}{E_0}\left(\frac{1}{\beta_+} + \frac{1}{\beta_-}\right) \tag{6}$$

where k is the Boltzman constant, E_0 is the activation energy of the dopant diffusion in the substrate, and β_+ and β_- are the heating and cooling rates, respectively. The correction term in (6) becomes negligible when t is large. For the heating and cooling rates used in this study, in the case of ZnO diffusion in lithium niobate the correction is negligible when t exceeds about 10 h.

To verify the applicability of this model to Zn-diffused waveguides, we compared the measured index profiles of six waveguides with profiles calculated as follows: 1) calculate the corrected diffusion coefficient D at the diffusion temperature from Table I, 2) calculate both the effective diffusion time t_{eff} (6) and t_1 (2), 3) calculate the dopant profile, using (1) if $t_{eff} < t_1$ or (4) if $t_{eff} > t_1$ (or (5) if $t_{eff} \geq 2t_1$), and 4) multiply the dopant profile by the $\Delta n/[Zn]$ factor (Table II) to obtain the index profile.

The waveguide mode effective indices and mode turning points were measured by prism coupling and IWKB analysis. In the IWKB analysis a curve fitting routine was used to fit the experimental index profile to either a erfc or a Gaussian (depending on whether t was smaller or larger than t_1) and determine the index at the surface. Error in the effective index measurement was ± 0.0003. For a typical three mode waveguide fabricated in this research, the uncertainty in the assignment of the surface index in IWKB analysis calculation and the mode turning points are about ± 0.0006 and ± 0.6 m, respectively.

Fig. 8 shows the measured index profile and the calculated index profiles for the extraordinary polarization of a waveguide in MgO:$LiNbO_3$. The fabrication conditions were 80-nm ZnO film diffused at 1000°C for 1 h in a x-cut sample. Including the finite ramping time, the effective diffusion time was calculated to be 72 min. The calculated value of t_1 (2) was 45 min. In this case, $t_2 = 72 - 45 = 27$ min. The solid and dashed lines in Fig. 8 represent the profiles calculated according to the exact solution (4) and the approximate solution (5), respectively. The agreement between the exact profile and the measured profile is reasonable. The measured index value at the surface is somewhat higher than predicted, which could be due to uncertainties in the measured value of $\Delta n/[Zn]$, as discussed in Section IV.

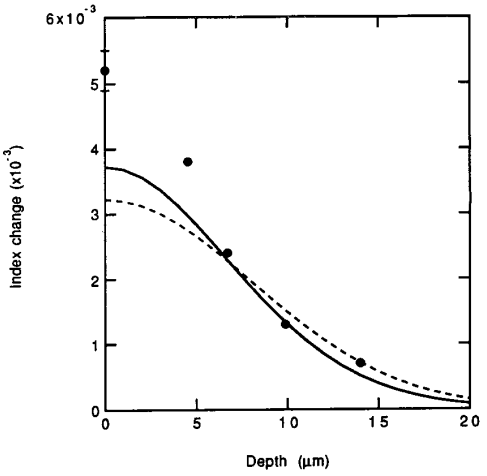

Fig. 8. Extraordinary index data measured by IWKB analysis on a waveguide fabricated in x-cut MgO:$LiNbO_3$ by diffusion of a 80-nm ZnO film at 1000°C for 1 h. The solid curve is the exact calculated profile (4) and the dotted line the approximate calculated profile (5).

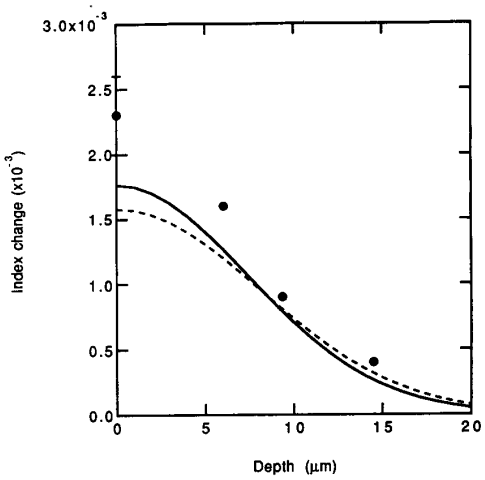

Fig. 9. Similar as Fig. 8, for z-cut $LiNbO_3$ (ordinary index data) after diffusion of a 100-nm ZnO film at 1000°C for 45 min.

Similar results are presented in Fig. 9 for a waveguide in $LiNbO_3$ (100-nm thick ZnO film, z-cut sample, 1000°C, 45 min). Including the finite ramping time, this corresponds to an effective diffusion time of 56.6 min. The calculated value of t_1 (2) was 23 min. In this case, $t_2 = 33$ min, the ratio $t_2/t_1 = 1.4$ is large enough that the exact profile resembles a Gaussian. Again the theoretical profiles are in reasonable agreement with the measured index profile.

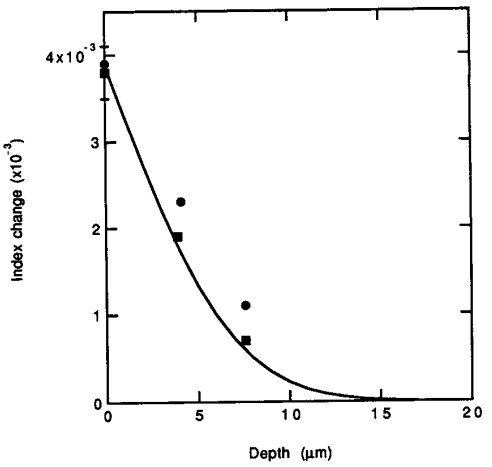

Fig. 10. Same as Fig. 9, with a diffusion time of 12 min. for two waveguides. Both waveguides were fabricated under the same conditions but in different runs. The solid curve is the calculated index profile calculated from (1).

Fig. 10 shows similar results for two waveguides as in Fig. 9 except that the diffusion time was decreased to 12 min. These two waveguides were fabricated under the same conditions but in different runs. Including the finite ramping time, the effective diffusion time was calculated to be 23.6 min. In this case $t_1 = 23$ min. so that the film was just depleted at the end of the diffusion process and (1) was used to generate the theoretical profile of Fig. 10. The surface index for the IWKB fit was determined by fitting to an erfc. For one of the waveguides the measured and calculated profiles agreed very well, to better than a few percent. For the second waveguide the agreement was fair; the actual profile depth was approximately 20% larger than the calculated depth.

The difference between the two data sets obtained from two different waveguides illustrates the limits of the reproducibility of our fabrication process. We believe this sample-to-sample variation is largely due to variations in film thickness. These variations change the total amount of Zn diffused into the sample, and therefore the total area under the index profile (see Fig. 10). Also, we speculate that film thickness variations may influence the total rate of Zn transport through the following process. While diffusion rate in single phase $LiNbO_3$ is similar for both thin and thick ZnO film samples, the initial kinetics associated with Zn dissolution into $LiNbO_3$ might require a period of time t_{sp}. In this ZnO-$LiNbO_3$ nonequilibrium system, t_{sp} may differ for films of different thickness. As discussed earlier, for typical diffusion times (30–60 min) this initial transient is not a significant rate limiting step and has a negligible effect on the final waveguide depth. However, in the case of the two waveguides of Fig. 10 the diffusion time was unusually short ($t = 12$ min), and the initial transient may influence the final waveguide depths. If t_{sp} depends on the film thickness, in this regime of very short diffusion times sample-to-sample variations in film thickness may lead to variations in waveguide depth (see Fig. 10)

The index profile is fairly sensitive to the fabrication conditions, so that the accuracy of our model in predicting a given waveguide profile is limited by the accuracy of the input parameters. For example, in the case of Fig. 9, a nearly perfect fit to the experimental profile is obtained when increasing the ZnO film thickness by 15% and decreasing the value of D by 15%. These variations are within the experimental errors in our measurements of these two quantities. The predictions of the model presented here should become more accurate when the process is better characterized.

Similar agreement was obtained for three other waveguides. Together with the examples illustrated in Figs. 8–10, these comparisons indicate that our model provides reasonable predictions of the index profile, generally within 40% for the surface index change and 20% for the 1/e depth. More detailed measurements are needed to refine the values of the model parameters, i.e., the diffusion coefficients and the $\Delta n/[Zn]$ coefficients.

VI. Conclusions

ZnO diffusion in MgO:$LiNbO_3$ and congruent $LiNbO_3$, and the index profile of waveguides fabricated by this process have been characterized. Earlier reports established the usefulness of this new type of waveguide, which guides both polarizations with low propagation losses and, in the case of MgO:$LiNbO_3$, exhibits high resistance to photorefractive damage. In the present study it was found that using ZnO instead of metallic zinc as a source and maintaining the ZnO film thickness below a prescribed value were important steps in avoiding second phase precipitation and maintaining the surface quality required for low loss waveguides. The refractive-index change produced by the Zn dopant varies approximately linearly with Zn concentration, with only a slight dependence on substrate orientation and diffusion temperature. Simple expressions from linear diffusion theory predict the waveguide index profile from the fabrication conditions. Comparison between calculated and measured profiles for a variety of waveguides showed that these model predictions are fairly accurate. Further studies of the dependence of the index change on Zn concentration and of the extraordinary index change in congruent $LiNbO_3$ are needed to improve the understanding of these waveguides. Diffusion studies using suitable dopant sources within the tie triangles containing $LiNbO_3$ can potentially provide useful information about the Zn transport. ZnO diffusion in lithium niobate appears to be an interesting process which has the potential to extend the spectrum of available waveguide devices.

Acknowledgment

The authors would like to thank Dr. Mei-Fan Sung Tang for helpful discussions, Crystal Technology for providing the crystals, and Lance Goddard for sputtering ZnO films. This work was supported by the NSF-MRL program through the Center for Materials Research at Stanford, and by Litton Systems, Inc.

References

[1] R. V. Schmidt and I. P. Kaminow, "Metal diffused optical waveguides," *Appl. Phys. Lett.*, vol. 25, pp. 458–460, 1974.

[2] J. L. Jackel, C. E. Rice, and J. J. Veselka, "Proton exchange for high-index waveguides in $LiNbO_3$," *Appl. Phys. Lett.*, vol. 41, pp. 607–608, 1982.
[3] S. K. Korotky and R. C. Alferness, in *Integrated Optical Circuits and Components,* L. D. Hutcheson, Ed. New York: Marcel Dekker, 1987, ch. 6, p. 215.
[4] R. A. Becker, "Thermal fixing of Ti-diffused $LiNbO_3$ channel waveguides for reduced photorefractive susceptibility," *Appl. Phys. Lett.*, vol. 45, pp. 121–123, 1984.
[5] M. M. Fejer, M. J. F. Digonnet, and R. L. Byer, "Generation of 22 mW of 532-nm radiation by frequency doubling in Ti:MgO:$LiNbO_3$ waveguides," *Opt. Lett.*, vol. 11, pp. 230–232, 1986.
[6] A. M. Glass, "The photorefractive effect," *Opt. Eng.,* vol. 17, pp. 470–479, 1978.
[7] G. Zhong, J. Jian, and Z. Wu, "Measurements of optically induced refractive damage of lithium niobate doped with different concentrations of MgO," in *Proc. 11th Int. Quantum Electron. Conf.* (Optical Society of America, Washington, D.C.), 1980, p. 631,
[8] J. Jackel *et al.,* "Damage-resistant $LiNbO_3$ waveguides," *J. Appl. Phys.*, vol. 55, pp. 269–270, 1984.
[9] G. E. Peterson, A. M. Glass, and T. J., Negran, "Control of the susceptibility of lithium niobate to laser-induced refractive index changes," *Appl. Phys. Lett.*, vol. 19, pp. 130–132, 1971.
[10] I. P. Kaminow and L. W. Stulz, "Nd:$LiNbO_3$ laser," *IEEE J. Quantum Electron.*, vol. QE-11, pp. 306–308, 1975.
[11] W. M. Young, R. S. Feigelson, M. M. Fejer, M. J. F. Digonnet, and H. J. Shaw, "Photorefractive damage resistant Zn-diffused waveguides in MgO:$LiNbO_3$," *Opt. Lett.*, vol. 16, 995–997, 1991.
[12] R. L. Holman, P. J. Cressman, and J. F. Revelli, "Chemical control of optical damage in lithium niobate," *Appl. Phys. Lett.*, vol. 32, pp. 280–283, 1978, Lindberg Furnace Company, Watertown, Wisconsin.
[13] D. W. Yoon and O. Eknoyan, "Characterization of vapor diffused Zn:LiTaO3 optical waveguides," *J. Lightwave Technol.*, vol. 6, pp. 877–880, 1988.
[14] V. B. Nalbandyan, B. S. Medvedev, V. I. Nalbandyan, and A. V. Chinenova, "Ternary system of niobium, zinc, and lithium niobate," *Inorganic Materials,* pp. 830–833, 1988.
[15] M. E. Villafuerte-Castrejon, A. Aragon-Pina, R. Valenzuela, and A. R. West, "Compound and solid-solution formation in the system Li_2O-Nb_2O_5-TiO_2," *J. Solid State Chem.*, vol. 71, pp. 103–108, 1987.
[16] M. N. Armenise *et al.,* "Characterization of TiO_2, LiNb3O8, and $(Ti0.65Nb0.35)O_2$ compound growth observed during Ti:$LiNbO_3$ optical waveguide fabrication," *J. Appl. Phys.*, vol. 54, pp. 6223–6231, 1983.
[17] C. E. Rice and R. J. Holmes, "A new rutile structure solid-solution phase in the LiNb3O8-TiO_2 system, and its role in Ti diffusion into $LiNbO_3$," *J. Appl. Phys.*, vol. 60, pp. 3836–3839, 1986.
[18] D. W. Yoon and O. Eknoyan, "Characterization of vapor diffused Zn:LiTaO3 optical waveguides," *J. Lightwave Technol.*, vol. 6, pp. 877–880, 1988.
[19] R. E. Hill, *Physical Metallurgy Principles, 2nd ed.* New York: Van Nostrand, 1973, ch. 6, 10, 11.
[20] J. M. White and P. F. Heidrich, "Optical waveguide refractive index profiles determined from measurement of mode indices: A simple analysis," *Appl. Opt.*, vol. 15, pp. 151–155, 1976.
[21] J. R. Carruthers, I. P. Kaminow, and L. W. Stulz, "Diffusion kinetics and optical waveguiding properties of outdiffused layers in lithium niobate and lithium tantalate," *Appl. Opt.*, vol. 13, pp. 2333–2342, 1974.
[22] C. R. Barrett, W. D. Nix, and A. S. Tetelman, *The Principles of Engineering Materials.* New Jersey: Prentice-Hall, 1973, p. 158, ch. 5.
[23] B. I. Boltaks, *Diffusion in Semiconductors.* New York: Academic, 1963, ch. 4, p. 102.
[24] See, for example, W. M. Young, Compositional Control by Diffusion in Lithium Niobate ($LiNbO_3$) for Optical Applications, Ph. D. dissertation, Stanford Univ., 1992.

W. M Young, photograph and biography not available at the time of publication.

M. M Fejer, photograph and biography not available at the time of publication.

M. J. F. Digonnet, photograph and biography not available at the time of publication.

A F. Marshall, photograph and biography not available at the time of publication.

R. S. Feilgelson, photograph and biography not available at the time of publication.